ACS APPLIED MATERIALS & INTERFACES

Research Article

www.acsami.org

Dynamic Biostability, Biodistribution, and Toxicity of L/D-Peptide-Based Supramolecular Nanofibers

Cuihong Yang,[‡] Liping Chu,[‡] Yumin Zhang,[‡] Yang Shi,[§] Jinjian Liu,[‡] Qiang Liu,[‡] Saijun Fan,[‡] Zhimou Yang,[§] Dan Ding,*[,§] Deling Kong,*[,§] and Jianfeng Liu*[,‡]

[‡]Tianjin Key Laboratory of Radiation Medicine and Molecular Nuclear Medicine, Institute of Radiation Medicine, Chinese Academy of Medical Science & Peking Union Medical College, Tianjin 300192, P. R. China

[§]State Key Laboratory of Medicinal Chemical Biology, Key Laboratory of Bioactive Materials, Ministry of Education, College of Life Sciences, and Collaborative Innovation Center of Chemical Science and Engineering (Tianjin), Nankai University, Tianjin 300071, P. R. China

Supporting Information

ABSTRACT: Self-assembling peptide nanofibers (including naturally L-amino acid–based and unnaturally D-amino acid–based ones) have been widely utilized in biomedical research. However, there has been no systematic study on their in vivo stability, distribution, and toxicity. Herein we systematically study the in vivo dynamic biostability, biodistribution, and toxicity of supramolecular nanofibers formed by Nap-GFFYGRGD (L-amino acid-based, L-fibers) and Nap-G^{D}F^{D}F^{D}YGRGD (D-amino acid–based, D-fibers), respectively. The D-fibers have better in vitro and in vivo biostabilities than L-fibers. It is found that D-fibers keep a good integrity in plasma during 24 h, while half of L-fibers are digested upon incubation in plasma for 6 h. The biodistributions of L- and D-fibers are also studied using the iodine-125 radiolabeling technique. The results reveal that L-fibers mainly accumulate in stomach, whereas D-fibers preferentially distribute in liver. Successive administrations of both L- and D-fibers with the dose of 30 mg/kg/dose cause no significant inflammation, liver and kidney function damages, immune reaction, and dysfunction of hematopoietic system. This study will provide fundamental guidelines for utilization of self-assembling peptide-based supramolecular nanomaterials in biomedical applications, such as drug delivery, bioimaging, and regenerative medicine.

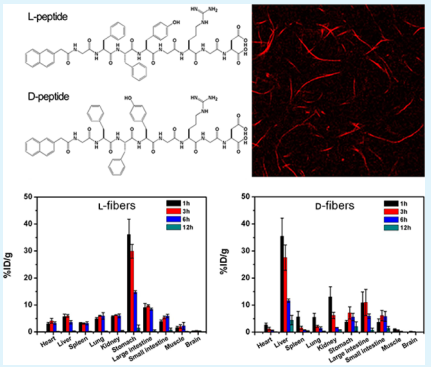

KEYWORDS: *self-assembling nanofibers, L/D-peptides, biodistribution, biostability, in vivo toxicity*

INTRODUCTION

Peptide-based nanomaterials have attracted intensive research interests in recent years because of the inherent properties of peptides including biocompatibility, degradability, bioactivity, fast stimuli-triggered responsiveness, as well as the ease of design and synthesis.[1−5] The nanomaterials are usually formed by the self-assembly of amphiphilic peptides or peptide derivatives via noncovalent interactions.[6−8] To date, there have been several kinds of well-known systems of self-assembling peptides as well as peptide derivatives being developed, which include amphiphilic peptides of RADA16,[9] Q11[10] and their analogues,[11,12] peptides functionalized with alkyl chains (e.g., peptide amphiphiles),[13] short peptides based on dipeptide of Phe-Phe (FF),[14,15] and short peptides with N-terminal aromatic capping groups.[16−18] These nanomaterials have shown great potential in a variety of biomedical applications such as sensing of biologically and environmentally important analytes,[19−21] three-dimensional (3D) cell culture,[18,22,23] delivery of therapeutic agents,[24−26] suppression of cancer cells and bacteria,[27−30] and regenerative medicine.[31−33]

The amphiphilic peptides and peptide derivatives are often capable of self-assembling into ordered nanostructures, such as nanofibers, nanotubes, or nanospheres.[34−36] They usually appear as supramolecular hydrogels at high concentrations and dispersions of nanomaterials at low concentrations. The supramolecular hydrogels are physical gels, which are able to be injected directly in subcutaneous spaces for topical treatments. Furthermore, the nanomaterial dispersions at low concentrations are suitable for intravenous (i.v.) administrations for therapeutic agent delivery.[37,38] Several groups have reported that peptide-based supramolecular hydrogels are biocompatible when administrated in subcutaneous spaces of mice. For examples, Stupp and co-workers have reported the in vivo dynamics of biocompatibility of peptide amphiphile hydrogels.[38] Xu's group has also compared the in vivo stability of α-amino acid- and β-amino acid–based peptide hydrogels.[39,40] Collier's group has reported that Q11 peptide possesses a low immunogenicity.[41,42] These results demonstrate that peptide-based supramolecular nanomaterials are biocompatible. However, the results also show that L-peptide-based materials are

Received: November 7, 2014
Accepted: January 2, 2015
Published: January 2, 2015

DOI: 10.1021/am507800e
ACS Appl. Mater. Interfaces 2015, 7, 2735−2744

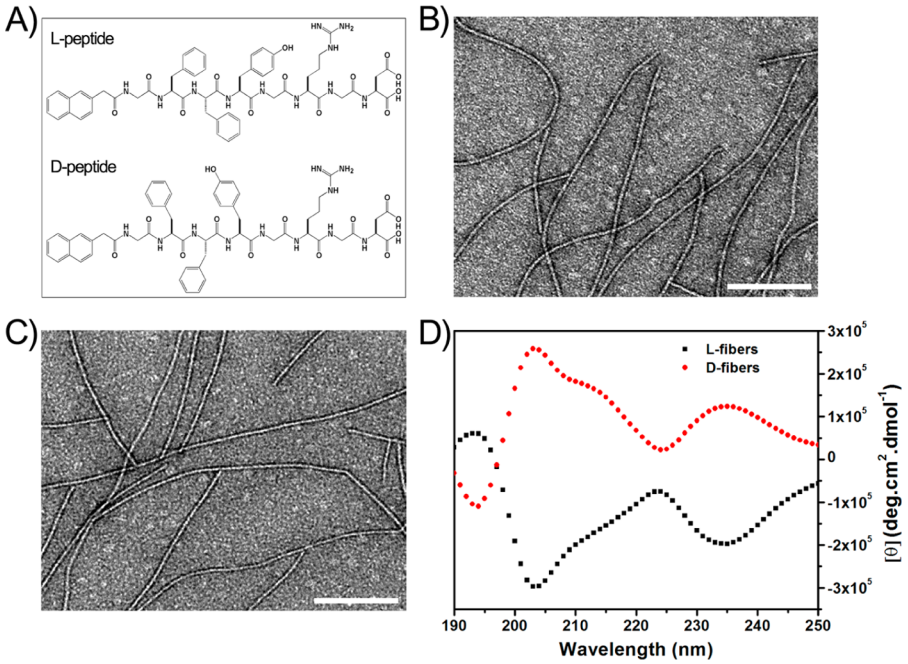

Figure 1. (A) Chemical structures of the L/D-peptides. Transmission electron microscope (TEM) images of (B) L-fibers and (C) D-fibers (scale bars represent 100 nm). (D) Circular dichroism spectra of L/D-fibers.

easily degradable.[39,43] For instance, the lifetime of hydrogels of Nap-FFY is shorter than 24 h in subcutaneous space of mice.[40] The utilization of D-amino acids in constructing such nanomaterials can moderately improve their biostability due to the lack of digestion enzymes in human body. Besides, one recent study reported by Xu's group shows that the integration of D-amino acids with a nonsteroid anti-inflammatory drug (NSAID) can boost the selectivity of the NSAID to cyclooxygenase-2 (COX-2) over COX-1.[44]

These pioneering works highlight the promising applications of D-amino acid–based nanomaterials for the delivery of therapeutic agents. However, the in vivo stability, biodistribution, as well as toxicity of the self-assembling L/D-peptides, especially when i.v. administrated, have not been studied and reported yet, which motivated us to perform such studies for offering useful and insightful information in future development and in vivo applications of L/D-peptide-based nanomaterials. Therefore, in this work, we investigated the in vivo dynamic biostability, biodistribution, and toxicity of supramolecular nanofibers formed by L- and D-peptides (Nap-GFFYGRGD and Nap-G^{D}F^{D}F^{D}YGRGD in Figure 1A), respectively. Noteworthy is that we studied and compared the stabilities of L- and D-peptide-based nanofibers in complex biological environments including blood plasma and in vivo circulating blood system for the first time. This study will provide fundamental guidelines for utilization of self-assembling peptide-based supramolecular nanomaterials in biomedical applications, such as drug delivery, bioimaging, and regenerative medicine.

MATERIALS AND METHODS

Materials and Animals. Fmoc-amino acids and Rink amide-AM resin were purchased from GL Biochem (Shanghai, China). Chemical solvents and reagents were purchased from Alfa (Shenzhen, China). Carbon-coated copper grids were obtained from Zhongjingkeyi Technology (Beijing, China). Nile Blue A was obtained from Alfa Aesar (Shanghai, China). Iodine-125 was purchased from PerkinElmer (California, USA). Roswell Park Memorial Institute 1640 Medium (RPMI-1640), fetal bovine serum (FBS) and other cells culture reagents were provided by Gibco (GrandIsland, USA). Other chemical solvents and reagents were of analytical or HPLC grade without further purification and obtained from Alfa (Shenzhen, China).

Four- to five-week-old healthy female BALB/c mice were obtained from Vital River Laboratories (Beijing, China) and fed in a germ-free environment. All the animal experiments were performed according to the protocol approved by IRM-CAMS.

Synthesis and Characterization of Peptide. The L/D-peptides of Nap-GFFYGRGD and Nap-G^{D}F^{D}F^{D}YGRGD were synthesized according to our previous reports.[45,46] Briefly, the L/D-peptides were synthesized by solid-phase peptide synthesis (SPPS) and then purified by high-performance liquid chromatography (HPLC, LUMTECH, Germany). The synthesized peptides were characterized by ^{1}H NMR (Bruker, Switzerland) and high-resolution mass spectrometry (HR-MS, England).

Nanofibers Formation and Morphological Characterization. L/D-peptide solutions were prepared at concentration of 3 mg/mL in PBS and then 2.0 equiv of Na_2CO_3 was added to adjust the pH of the solutions to 7.4, respectively. L/D-fibers would form during the cooling process after being boiled. Morphologies of the L/D-fibers self-assembled by L/D-peptides were characterized by transmission electron microscope (TEM, JEOL, Japan) at 200 kV. Specifically, 10 μL of the L/D-fibers samples were dropped on a copper grid and incubated for 60 s and then rinsed with deionized water twice. Ten microliters of the saturated uranyl acetate solution was dropped onto the sample plate for 10 s and then rinsed with deionized water twice. The sample plates were kept overnight before the measurement.

Circular Dichroism Spectroscopy. L/D-Fibers were prepared in PBS solution at the concentration of 2 mg/mL. 500 μL of the sample was added into a circular dichroism (CD) cuvette with a 2 mm path-length. Measurements were performed on a CD spectrometer (JASCO Corp., J-810, Japan) from 190 to 250 nm.

Biostability of L/D-Fibers in Vitro and in Vivo. To study the biostability of nanofibers in plasma, L/D-fibers were stained with Nile Blue A. Briefly, Nile Blue A powder was dissolved in deionized water at concentration of 1 mg/mL. Nile Blue A solution (10 μL) was added into peptide solution (500 μL, 3 mg/mL). Nile Blue A-stained nanofibers would form during the cooling process after being boiled. For in vitro biostability study, plasma was prepared by collecting whole blood of healthy mice into heparinized tube and centrifugation at 3500

DOI: 10.1021/am507800e
ACS Appl. Mater. Interfaces 2015, 7, 2735−2744

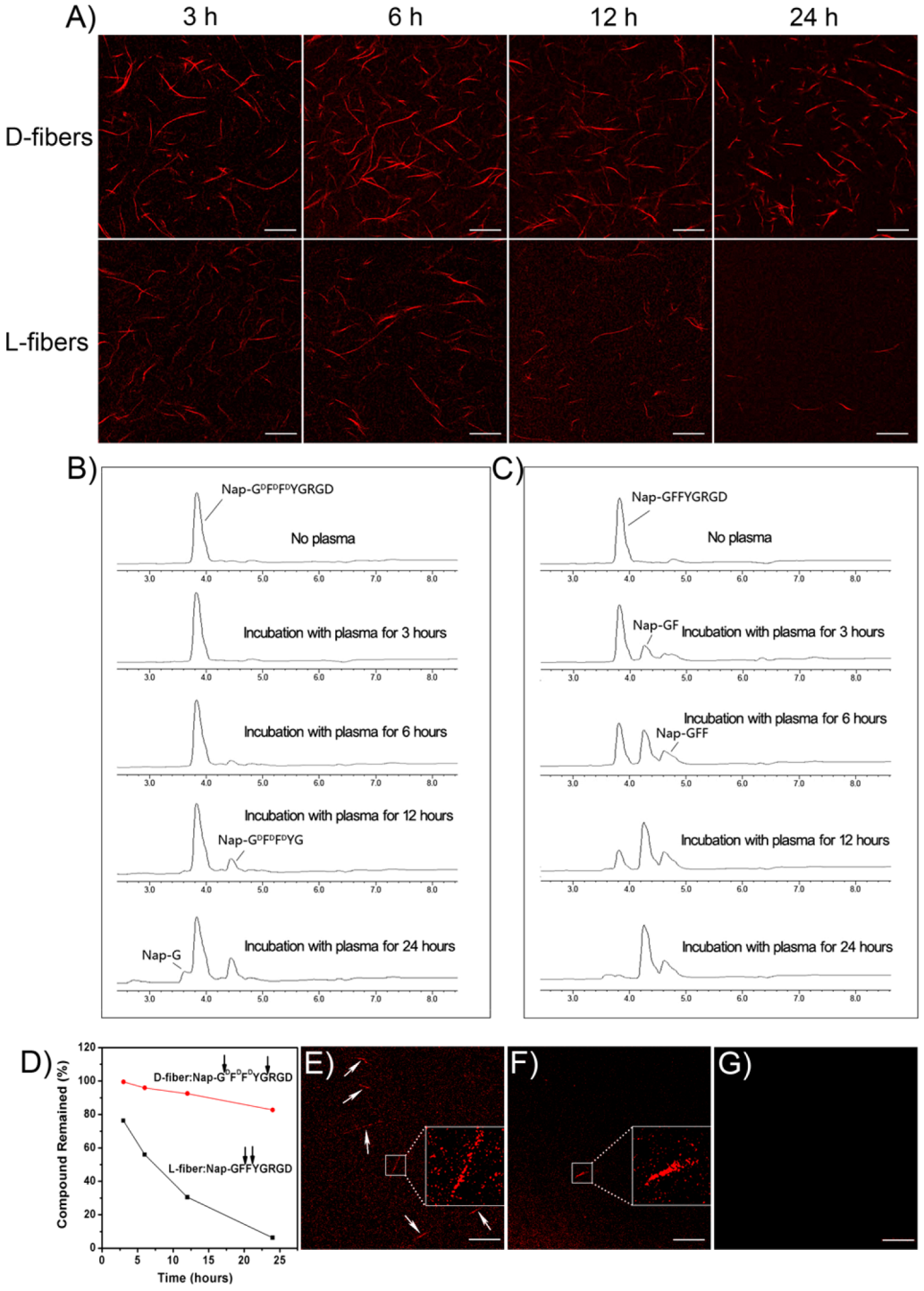

Figure 2. (A) Time-dependent CLSM images of D- and L-fibers in blood plasma. LC-MS traces of (B) D- and (C) L-peptides incubated in blood plasma at different time points. (D) Quantitative analysis of the LC-MS data in B and C. CLSM images of D-fibers observed in the in vivo blood circulation at (E) 0.5 h and (F) 1 h post i.v. injection. (G) CLSM image of L-fibers observed in the in vivo blood circulation at 0.5 h post i.v. injection. All scale bars in A, E–G represent 25 μm.

rpm for 10 min. Nile Blue A-stained L/D-fibers were incubated in plasma at concentration of 0.5 mg/mL at 37 °C for 3 h, 6 h, 12 and 24 h, respectively. Fluorescence images of Nile Blue A-stained L/D-fibers were taken by confocal laser scanning microscopy (CLSM, TCS SP5, Leica, Germany) at the designated time points. For in vivo biostability study, 200 μL of Nile Blue A-stained L/D-fibers were administrated in the mice via the tail vein at a dose of 30 mg/kg body weight. Blood sample was collected from eyes at 0.5 h, 1 and 6 h, respectively. For CLSM observation, blood cells were removed from the sample by centrifugation at 3500 rpm for 10 min.

To quantitatively study the degradation rate of the L/D-peptides and the degradation sites in vitro and in vivo, the samples were also analyzed by LC-MS (LCMS-2020, Japan). For sample preparation, 4-fold volume of acetonitrile was added to the incubated plasma sample, votexed, and centrifugated at 12000 rpm at 4 °C for 10 min to sediment the protein impurities.

DOI: 10.1021/am507800e
ACS Appl. Mater. Interfaces 2015, 7, 2735–2744

Radiolabeling of L/D-Peptides by Iodine-125 (^{125}I). L/D-Peptides were labeled with ^{125}I on the tyrosine residue of the peptide using chloramine-T method. Briefly, Na^{125}I (0.5 mCi) in 10 mM PBS was added to L- or D-peptide solution in PBS (3 mg/mL). The reaction was done at 20 °C for 5 min. Then, 100 μL of sodium peroxodisulfate was added to quench the reaction. The labeling rate and radiochemical purity of the peptides were detected by radioactive thin-layer chromatography (TLC) scanner (BioScan, America). The mobile phase was 10% deionized water and 90% ethanol. The unreacted ^{125}I and other chemicals were removed by radioactive HPLC (Dionex UltiMate3000, America).

Biodistribution of L/D-Fibers. Healthy BALB/c mice were intravenously administrated with ^{125}I-labeled L- and D-fibers (3 mg/mL), respectively, on the basis of radiation dose of 1.85×10^4 Bq/g body weight (n = 4 mice for each nanofiber). At designated time points (1, 3, and 12 h), the mice were anesthetized and imaged by planar Gamma camera (KODAK IS in vivo FX; Kodak). At 1 h postinjection, the mice treated with ^{125}I-labeled L- and D-fibers, respectively, were sacrificed and the tissues including liver, heart, stomach, spleen, lung, kidney, and intestine were taken for ex vivo imaging. For the quantitative biodistribution study, the healthy mice were randomly divided into two different groups (12 mice per group with three mice per time point) and intravenously injected with ^{125}I-labeled L- and D-fibers (3 mg/mL), respectively, on the basis of radiation dose of 1.85×10^4 Bq/g body weight. At designated time points (1, 3, 6, and 12 h), the mice were sacrificed and main tissues and organs including heart, liver, spleen, lung, kidney, stomach, small intestine, large intestine, skeletal muscle, and brain were harvested and weighed (small intestine, large intestine, and stomach were emptied and washed with saline first). The radioactivity of tissue samples was detected by γ-counter (2470 WIZARD,[2] PerkinElmer, America). The quantitative data of organ distribution were presented with percentage of injected dose per gram of tissue/organ (%ID/g). All data were corrected to account for decay.

Animal Injection and Dose Selection. Mice were randomly divided into five groups (12 mice per group with four mice per time point): PBS, L-fibers-10, L-fibers-30, D-fibers-10, and D-fibers-30. Ten and 30 represent the injection dose of 10 and 30 mg/kg, respectively. L- or D-fibers solution (2 mg/mL) was prepared as above-described and was diluted by PBS into 300 μL on the basis of nanofibers concentrations of 10 and 30 mg/kg body weight, respectively. PBS or the diluted samples was administrated via the tail vein once a day for five total administrations.

Hematology and Biochemistry Analysis. Hematological and biochemical examination were performed by automatic blood analyzer (Celltace, Japan) and automatic biochemical analyzer (Vitalab, Holland). Hematological and biochemical analysis were performed at 1 day after the first administration (D1), 1 day after five successive administrations (D5, the i.v. treatment of L- or D-fibers was performed every day from D0 to D4) and 1 week after the five successive administrations (D11). The whole blood samples were collected from eyes at the designated time points. Briefly, 100 μL of blood sample was collected into heparinized tube for hematological analysis. 500 μL of blood sample was collected into a 1.5 mL centrifuge tube and serum was harvested by centrifugation at 3500 rpm for 10 min for biochemical analysis.

Body Weight, Immune Response, and Histology Evaluation. Mouse weight was monitored upon the first injection. To study the immune response of the experimental mice, spleen and thymus were harvested and weighed at the designated time points (D1, D5, and D11) after blood was collected. The spleen and thymus index were calculated as the ratio of tissue weight (mg) to body weight (g). In order to evaluate the toxicity of nanofibers in mice after successive intravenous injections, histology studies were also performed at D5 and D11. Specifically, liver, spleen, kidney, and stomach were harvested and fixed immediately in 4% paraformaldehyde for 24 h. Haematoxylin & eosin (H&E) assays were performed according to the standard protocols.

Statistical Analysis. The data were presented as mean ± standard deviation. An independent t test was used for the statistical analysis performed with SPSS 19. *$p < 0.05$ was considered to have statistical significance.

RESULTS AND DISCUSSION

Synthesis and Characterization of L/D-Peptide-Based Nanofibers. The L- and D-peptides of Nap-GFFYGRGD and Nap-G^{D}F^{D}F^{D}YGRGD were synthesized by standard solid-phase 9-fluorenylmethoxycarbonyl (Fmoc) peptide chemistry, according to our previous report.[45] The chemical structures of the L/D-peptides are shown in Figure 1A. Both the L/D-peptides exhibit good self-assembling capabilities, which are able to form supramolecular nanofibers (L-fibers and D-fibers, respectively), verified by the TEM observation. The TEM images shown in Figure 1B, C indicate that the L- and D-fibers formed by Nap-GFFYGRGD and Nap-G^{D}F^{D}F^{D}YGRGD, respectively, have similar morphology with length of micrometer levels and an average width of approximately 16 nm. The secondary structures of the L-fibers and D-fibers were then studied by CD spectroscopy. The CD spectra shown in Figure 1D indicate that both L- and D-fibers have a stable α-helix secondary structure in the PBS buffer solution, and the mirror pattern of L-fibers and D-fibers reflects their chirality.

Biostabilities in Blood Plasma and In Vivo Circulating System. After preparation of the L- and D-fibers, the dynamic biostabilities in blood plasma and in vivo circulating system were estimated. The supramolecular L- and D-fibers were stained with Nile Blue A in order to be visualized under the CLSM observation. The Nile Blue A was selected to stain the nanofibers because it was reported to be very effective and widely utilized in staining self-assembled nanostructures.[47] The Nile Blue A-stained L- and D-fibers were first added to mouse blood plasma in vitro, which was followed by imaging with CLSM at designated time intervals. The images in Figure 2A indicate that although the density of fluorescent D-fibers becomes slightly lower and their length changes a bit shorter as the time elapses, a large number of D-fibers can still be clearly observed even after 24 h incubation with plasma. In comparison, the density of fluorescent L-fibers remarkably decreases and their length becomes to be very short with the prolonged incubation time. Only very few L-fibers can be observed after 24 h incubation with plasma (Figure 2A). The biostabilities of L- and D-fibers in blood plasma were also assessed by LC-MS. As shown in Figure 2B, C as well as Figures S2 and S3 in the Supporting Information, the enzymatic degradation sites of Nap-G^{D}F^{D}F^{D}YGRGD and Nap-GFFYGRGD are the carboxy terminal of Glycine (G) and the carboxy terminal of Phenylalanine (F), respectively. Overall, according to the LC-MS data, upon incubation in plasma for 24 h, more than 95% of L-fibers are digested, whereas only around 17% of D-fibers are degraded (Figure 2D). The LC-MS results suggest that the reduced density and length of fluorescent L/D-fibers in blood plasma observed by CLSM should be due to the digestion of peptides. Both the CLSM and LC-MS data illustrate that D-fibers from self-assembling D-peptides possess much better biostability in plasma as compared to their L-counterparts.

Furthermore, the in vivo biostabilities of L- and D-fibers in circulating blood system were also studied. In this experiment, Nile Blue A-stained L- and D-fibers at a concentration of 3 mg/mL were i.v. injected into the healthy mice, respectively. At designated time intervals, 500 μL of mouse blood was collected, centrifugated, and imaged by CLSM. As shown in Figure 2E, F, a number of fluorescent D-fibers can be clearly observed in the

DOI: 10.1021/am507800e
ACS Appl. Mater. Interfaces 2015, 7, 2735−2744

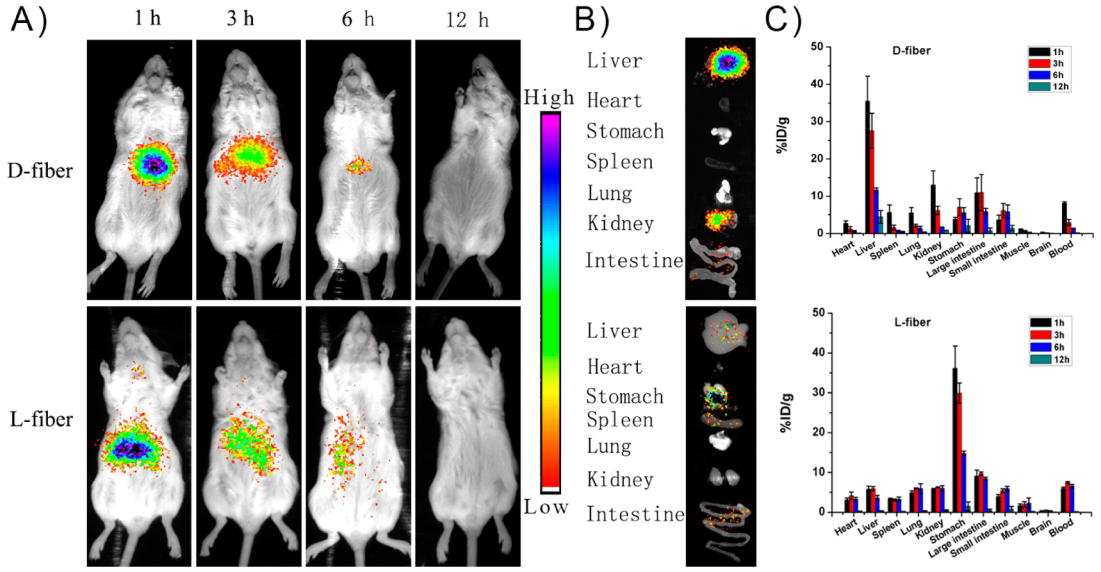

Figure 3. (A) In vivo noninvasive Gamma camera images of the BALB/c mice after intravenous administration with ^{125}I-labeled L- and D-fibers, respectively, for designated time intervals. (B) Ex vivo imaging of various tissues. The mice treated with ^{125}I-labeled L- and D-fibers, respectively, were sacrificed at 1 h postinjection and the indicated tissues were collected for ex vivo imaging. (C) Quantitative biodistribution of ^{125}I-labeled L- and D-fibers in mice. Tissues were harvested and weighted at 1, 3, 6, and 12 h after initial injection of BALB/c mice, respectively. Data were presented as percent injected dose per gram (%ID/g) ± standard deviation, n = 3.

blood circulation at the initial time points post injection. However, the fluorescent D-fibers seem to disappear in the blood circulation under CLSM observation after 6 h administration (Figure S1A in the Supporting Information). This should be because of several factors including the high autofluorescence of blood, the degradation of D-fibers and the uptake of nanofibers by reticuloendothelial system (RES) and mononuclear phagocyte system (MPS) tissues. In comparison, few L-fibers can be observed even at 0.5 h post injection (Figure 2G). Moreover, the LC-MS was also employed to determine the digestion of D- and L-fibers in the blood circulation in vivo. The results are depicted in Figures S4−S7 in the Supporting Information, which reveal the faster degradation of both L- and D-fibers in blood circulation in vivo than in plasma in vitro. These data together also indicate that D-fibers have better in vivo biostability as well as longer blood circulation time as compared to L-fibers.

In Vivo Biodistribution. To investigate the fate of L- and D-fibers in vivo after i.v. administration, radioactive tracing technique was employed, as this technique is straightforward and highly sensitive to probe quantitatively the in vivo behavior. In this study, L- and D-fibers were radiolabeled with radioactive nuclide, iodine-125 (^{125}I) by the reaction between ^{125}I and the tyrosine (Y) residue of Nap-GFFYGRGD and Nap-G^{D}F^{D}F^{D}YGRGD, respectively. The HPLC could efficiently purify the radiolabeled L- and D-peptides, and the radiochemical purity of ^{125}I-labled L- and D-peptides was measured to be higher than 99%, respectively (Figures S8 and S9 in the Supporting Information). Moreover, both the ^{125}I-labeled L- and D-peptides possess good in vitro radiolabel stabilities, as evidenced by the >90% of the radiochemical purity after 72 h incubation of the radiolabeled peptides in blood plasma (Figure S10 in the Supporting Information). Figure 3A exhibits the noninvasive Gamma camera images of the healthy BALB/c mice after i.v. administration with ^{125}I-labeled L- and D-fibers for 1, 3, 6, and 12 h, respectively. For both nanofibers, the radioactive signals are enriched in the mouse abdomen area and significantly decrease over time. Additionally, at 1 h post injection of ^{125}I-labeled L- and D-fibers, respectively, the mice were sacrificed and the main tissues were conducted for ex vivo imaging (Figure 3B). Furthermore, upon i.v. injection of ^{125}I-labeled L- and D-fibers into the healthy mice, respectively, their in vivo time-dependent biodistribution were also quantitatively determined by a Gamma counter (Figure 3C). The results in Figure 3B, C indicate the dramatically different biodistributions between ^{125}I-labeled L- and D-fibers. In detail, the L-fibers are preferentially distributed in the digestive system and there are the highest radioactive signals in the stomach tissue. On the other hand, the D-fibers are mainly accumulated in liver tissue, followed by kidney and large intestine. It should be noted that almost no radioactive signals can be detected post 12 h injection for both L- and D-fibers, indicating both nanofibers are able to be quickly cleared from the body. This result agrees well with those depicted in Figure 2E, F and Figure S1A in the Supporting Information, which reveal that the fluorescent D-fibers can be clearly observed in the blood circulation at 0.5 and 1 h postinjection, but nearly disappear from the blood after 6 h administration. The fast metabolic character of self-assembling L/D-peptides implies that they would not long-term accumulate in the body, resulting in cumulative toxicities, which could thus be applied as successive i.v. injected biomedical nanomaterials.[48,49]

It is important to note that after i.v. administration of ^{125}I-labeled L- and D-fibers, respectively, there are very few detectable signals from the thyroids of both L- and D-fiber treated mice within the tested time period (12 h after injection), as depicted in Figure 3A. As it is well-known that the free ^{125}I would mainly accumulate in both the thyroid and gastrointestinal tract,[50] this result indicates that the enrichment of ^{125}I-labeled L-fibers in the stomach tissue is not ascribed from the dehalogenation of the labeled L-peptides. On the basis of the results in Figure 2, the L-fibers would be quickly digested after i.v. injection. Actually, the materials accumulated in the stomach are not the intact L-fibers or L-peptides, but the ^{125}I-

DOI: 10.1021/am507800e
ACS Appl. Mater. Interfaces 2015, 7, 2735−2744

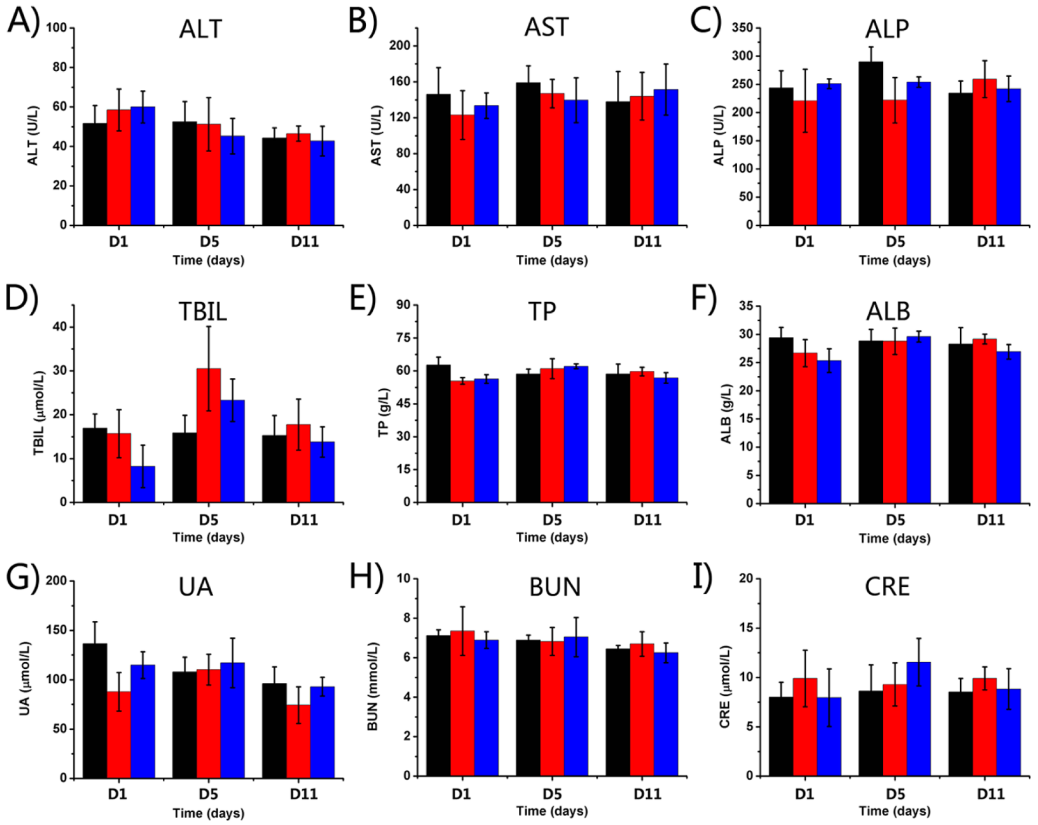

Figure 4. Blood biochemistry data of mice exposed to the i.v. injection of D-fibers and L-fibers of 30 mg/kg/dose, respectively. These results show mean ± standard deviation (n = 4) of (A) alanine transaminase (ALT), (B) aspartate transaminase (AST), (C) alkaline phosphatase (ALP), (D) total bilirubin (TBIL), (E) total protein (TP), (F) albumin (ALB), (G) urea (UA), (H) blood urea nitrogen (BUN) and (I) creatinine (CRE). Black column represents the PBS control group; red column represents the L-fiber group and blue one represents D-fiber group. D1, D5, and D11 represent 1 day after the first i.v. injection, 1 day after five successive i.v. injections, and 1 week after five successive i.v. injections, respectively.

labeled L-peptide residues after degradation in vivo. On the other hand, the D-fibers have better in vivo biostability as well as longer blood circulation as compared to L-fibers. Although D-fibers would also experience degradation in vivo, they still maintain the nanofiber structures, which make them preferentially enriched in the reticuloendothelial system (RES) organs, especially the liver tissue.[51]

In Vivo Toxicity Study. Although there have been a number of reports regarding to the application of peptide-based supramolecular nanofibers with i.v. injection,[36,52−54] none of them systematically studied the in vivo toxicity of these peptide-based nanofibers, especially those containing non-natural D-amino acids. Therefore, in this work, we systematically investigated and compared the in vivo toxicities of the L- and D-fibers self-assembled by Nap-GFFYGRGD and Nap-$G^DF^DF^DYGRGD$. In this experiment, L- or D-fibers at dose of 10 and 30 mg/kg were i.v. injected into the healthy mice, respectively. The nanofiber concentrations of 10 and 30 mg/kg/dose were used in this study, because when the concentration of both nanofibers is higher than 3.5 mg/mL (about 50 mg/kg/dose), the nanofiber solution becomes viscous, which is not suitable for utilization in i.v. injection. It is noted that the injection dose of peptide nanofibers for in vivo cancer drug delivery by Stupp's group was around 20 mg/kg,[26] the injection dose of carbon nanotubes for in vivo fluorescence imaging by Dai's group was about 3.5 mg/kg,[55] and the injection dose of liposome for in vivo cancer drug delivery by Lai's group was about 6.7 mg/kg.[56] Our setting of 30 mg/kg injection dose is much higher than these nanostructures for in vivo applications. The serum biochemistry, hematology, immune response and histology detections were conducted at 1 day after the first administration (D1), 1 day after five successive administrations (D5, the i.v. treatment of L- or D-fibers was performed every day from D0 to D4), and 1 week after the five successive administrations (D11). D1 represented single administration toxicity of fibers, D5 represented accumulative toxicity of fibers, while D11 represented the recovery of mice after successive administrations.

To monitor any potential toxic effects of the L- or D-fibers on BALB/c mice, we selected standard biochemistry indicators including alanine transaminase (ALT), alkaline phosphatase (ALP), aspartate transaminase (AST), total protein (TP), total bilirubin (TBIL), albumin (ALB), urea (UA), creatinine (CRE), and blood urea nitrogen (BUN) to study the effects of the supramolecular nanofibers on liver and kidney functions of mice. The levels of ALT and AST reflect the damage of liver parenchyma. TP and ALB are commonly used as the markers for the synthetic function of liver, wheras the ALP and TBIL reflect the bilirubin metabolism function of liver. All of the above indicators of L- and D-fiber-treated groups appear to be normal compared with PBS control group (Figure 4A−F and Figure S11A-F in the Supporting Information), indicating no liver injuries when treatments of mice with 10 mg/kg/dose (Figure S11A-F in the Supporting Information) and 30 mg/kg/dose (Figure 4A−F) of D-fibers and L-fibers at all of the tested time points. Moreover, the urea concentrations in the blood indicate the general conditions of liver and kidney. The higher concentrations of urea in the blood than the normal

DOI: 10.1021/am507800e
ACS Appl. Mater. Interfaces 2015, 7, 2735−2744

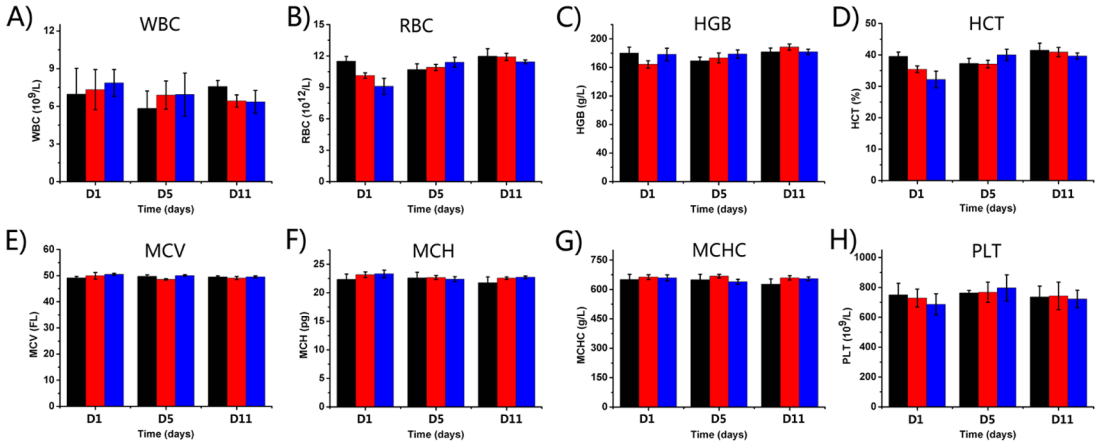

Figure 5. Hematology results of mice exposed to the i.v. injection of D-fibers and L-fibers of 30 mg/kg/dose. These results show mean ± standard deviation (n = 4) of (A) white blood cells (WBC), (B) red blood cells (RBC), (C) hemoglobin (HGB), (D) hematocrit (HCT), (E) mean corpuscular volume (MCV), (F) mean corpuscular hemoglobin (MCH), (G) mean corpuscular hemoglobin concentration (MCHC) and (H) platelet (PLT). Black column represents the PBS control group; red column represents the L-fiber group and blue one represents D-fiber group.

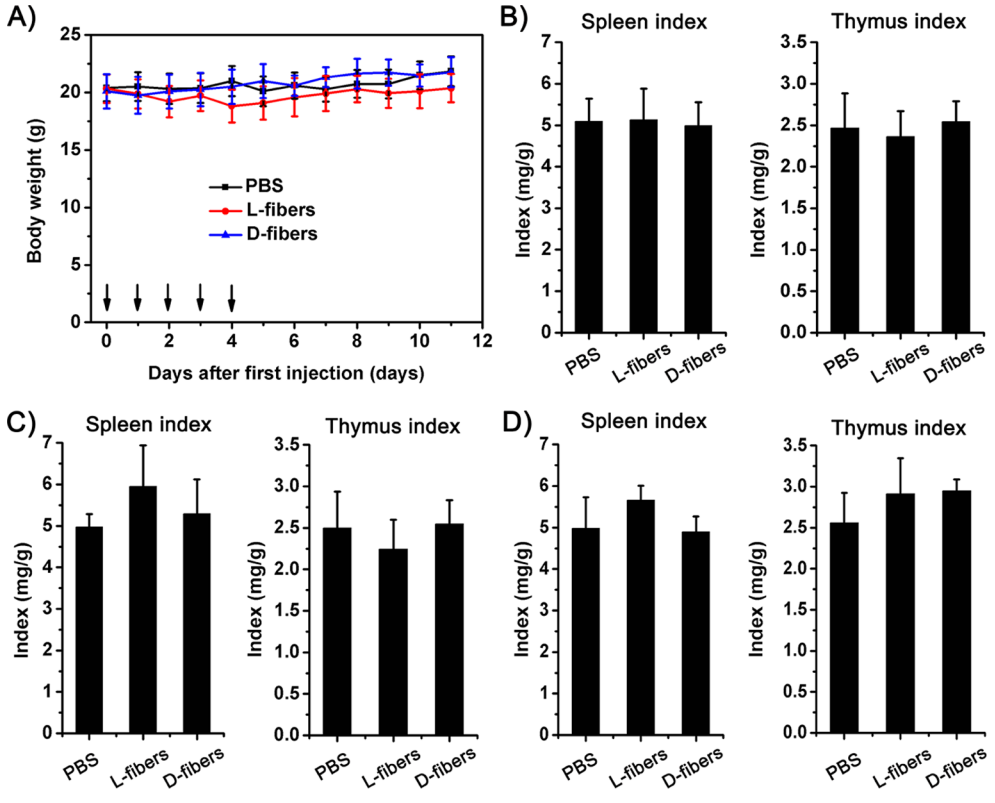

Figure 6. (A) Body weight changes of mice with various treatments (30 mg/kg/dose for L- and D-fibers). Spleen index and thymus index of 30 mg/kg/dose L-fiber and D-fiber-treated mice on (B) D1, (C) D5, and (D) D11. Data were expressed as mean ± standard deviation (n = 4).

concentration indicated disorder or damage to the renal function, while the lower concentrations reflect diseases or damage of liver.[57] As shown in Figure 4G–I and Figure S11G–I in the Supporting Information, All of the UA, BUN, and CRE levels are similar to those of control group when mice were treated with 10 mg/kg/dose (Figure S11G–I in the Supporting Information) and 30 mg/kg/dose (Figure 4G-I) of D-fibers and L-fibers at all of the detection time points, revealing that there are no kidney injuries. These results together suggest that the successive i.v. injections of L- or D-fibers at the above doses have no impairment on liver and kidney functions of mice.

Certain nanomaterials can induce hemolysis by damaging red blood cells (RBC), leucopenia by damaging white blood cells (WBC) or thrombus formation by causing platelet aggregation.[58] In our study, the standard hematology markers were also detected, such as WBC, RBC, hematocrit (HCT), hemoglobin (HGB), mean corpuscular hemoglobin (MCH), mean corpuscular volume (MCV), mean corpuscular hemoglobin concentration (MCHC), and platelets (PLT). The WBC is sensitive to the physiological response and usually elevates if there is inflammation. As shown in Figure S12 in the Supporting Information and Figure 5, upon treatments of mice with 10 and 30 mg/kg/dose of L- and D-fibers,

DOI: 10.1021/am507800e
ACS Appl. Mater. Interfaces 2015, 7, 2735–2744

respectively, all of the hematology markers show no significant differences as compared to those for PBS treatment on D1, D5 and D11. These results also reveal that L- and D-fibers do not cause inflammatory responses in main organs and have no side effects on the hematopoietic cells of spleen.

The body weight and immune response were studied as well. Figure 6A and Figure S13 in the Supporting Information show the changes of body weight of mice treated with 30 mg/kg/dose and 10 mg/kg/dose of fibers. During the study period, the administrations of L- or D-fibers would not bring statistical changes of mouse body weight, and we have not observed abnormal behaviors of mice. These results indicate that both L- and D-fibers possess no obvious adverse effects on the growth of mice. The spleen and thymus indexes were also calculated to reflex the immune response of mice to the fibers (Figure 6B–D and Figure S14 in the Supporting Information). There are no significant differences between the fiber groups and PBS group, indicating that the administrations of L- or D-fibers would not elicit immune response of mice. Collier and co-workers reported that peptide nanofibers composed of natural L-amino acids had minimal immunogenicity in mice.[59] Our results verified their conclusions and we also found that our D-peptide-based supramolecular nanofibers also exhibited minimal immunogenicity. These observations highlight the great promising biomedical applications of the supramolecular nanofibers of D-peptides.

To further study the in vivo toxicity of supramolecular nanofibers, histology evaluation was carried out by the hematoxylin and eosin (H&E) staining. The main metabolic organs of liver, kidney, and spleen were selected. Stomach was also included in the histology test because of the high accumulation of L-fiber in this tissue regarding to the biodistribution studies. All the H&E-stained tissue slices were estimated by 3 independent pathologists who were blinded to the project. The results depicted in Figure 7 and Figure S15–17 in the Supporting Information show that no apparent histopathological abnormalities and lesions can be observed for the groups treated with 10 or 30 mg/kg/dose L-fiber and D-fiber compared with the PBS control group on D5 and D11. The structures of red pulp and white pulp in the spleen are clear and

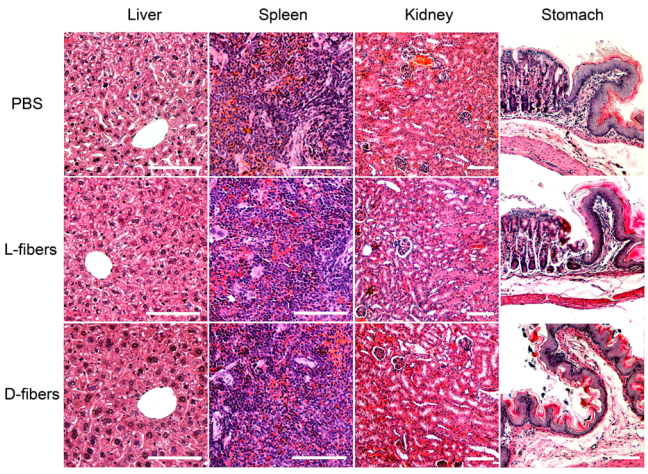

Figure 7. Haematoxylin & eosin (H&E) stained tissue slices (liver, spleen, kidney, and stomach) from mice treated with 30 mg/kg/dose of L-fibers and D-fibers on 1 day after five successive administrations (D5, the i.v. treatment of L- or D-fibers was performed every day from D0 to D4). The scale bar is 100 μm for all the images.

the proliferation of hematopoietic cells (granulocytes, erythrocyte, and megakaryocytes) are active in all of the L-fiber, D-fiber, and control groups on D5 and D11. The results also suggest that the L- or D-fibers have no obvious toxicities to the hematopoietic cells in spleen, which is consistent with the results obtained by the hematology studies and the normal of the spleen index. The hepatocytes in the liver and glomerulus structure in the kidney can be observed, which show normal structures compared with PBS groups. Also there are no injury and infiltration of inflammatory cells to the liver and kidney for all of the treatment groups, revealing that L- and D-fibers exhibit little or no toxicities to both the liver and kidney organs. This result agrees well with the blood biochemistry results. Furthermore, although L-fibers experience high accumulation in the stomach, there are no structure change of gastric mucosa and invasions of inflammatory in L-fiber group compared with the other treatment groups. Therefore, it is reasonable to conclude that the successive administrations of both L- and D-fibers would not cause inflammation and significant structural damage of mice.

CONCLUSIONS

In summary, we studied the in vitro and in vivo stabilities of supramolecular nanofibers with L- and D-amino acids. The results indicate that D-fibers possess better stabilities compared with L-fibers. The D- and L-fibers exhibit different biodistributions upon i.v. injection probably due to their different in vivo stabilities. The results of blood biochemistry, hematology, body weight, immune response, and histology reveal that successive i.v. administrations of L- or D-fibers would not cause obvious tissue dysfunction or damage, inflammatory response, dysfunction of hematopoietic system, and immune response. These observations suggest the good biocompatibilities of both D- and L-fibers under the tested concentrations. This is the first example of detailed in vivo stability, biodistribution, and biocompatibility of supramolecular nanofibers. Noteworthy is that both L- and D-fibers would be degraded easily and therefore would not cause significant toxicities to mice, suggesting their great potential in biomedical applications. We believe that this study will inspire more exciting research in the self-assembling peptide field.

ASSOCIATED CONTENT

Supporting Information

Biostability in circulating blood system, LC-MS analysis of degradation of L/D-fibers in vivo, radiochemical purity and in vitro stability analysis, hematology and biochemistry analysis, body weight, immune response and pathology evaluation. This material is available free of charge via the Internet at http://pubs.acs.org.

AUTHOR INFORMATION

Corresponding Authors

*E-mail: dingd@nankai.edu.cn.
*E-mail: kongdeling@nankai.edu.cn.
*E-mail: lewis78@163.com.

Notes

The authors declare no competing financial interest.

ACKNOWLEDGMENTS

We acknowledge the financial supports from NSFC (51303213, 81171371, 81301311 and 51203189), program for Changjiang

DOI: 10.1021/am507800e
ACS Appl. Mater. Interfaces 2015, 7, 2735–2744

Scholars and Innovative Research Team in University (IRT13023), Tianjin Science Foundation (13JCZDJC28100), PUMC Youth Fund and the Fundamental Research Funds for the Central Universities (3332014003, 33320140034) and the Development Foundation of IRM-CAMS (SF1417 and SF1416).

REFERENCES

(1) Collier, J. H.; Rudra, J. S.; Gasiorowski, J. Z.; Jung, J. P. Multi-Component Extracellular Matrices Based on Peptide Self-Assembly. *Chem. Soc. Rev.* **2010**, *39*, 3413−3424.
(2) Gao, Y.; Zhao, F.; Wang, Q.; Zhang, Y.; Xu, B. Small Peptide Nanofibers as the Matrices of Molecular Hydrogels for Mimicking Enzymes and Enhancing the Activity of Enzymes. *Chem. Soc. Rev.* **2010**, *39*, 3425−3433.
(3) Suzuki, M.; Hanabusa, K. L-Lysine-Based Low-Molecular-Weight Gelators. *Chem. Soc. Rev.* **2009**, *38*, 967−975.
(4) Zhao, X.; Zhang, S. Molecular Designer Self-Assembling Peptides. *Chem. Soc. Rev.* **2006**, *35*, 1105−1110.
(5) Zelzer, M.; Ulijn, R. V. Next-Generation Peptide Nanomaterials: Molecular Networks, Interfaces and Supramolecular Functionality. *Chem. Soc. Rev.* **2010**, *39*, 3351−3357.
(6) Ulijn, R. V.; Smith, A. M. Designing Peptide Based Nanomaterials. *Chem. Soc. Rev.* **2008**, *37*, 664−675.
(7) Ryan, D. M.; Nilsson, B. L. Self-Assembled Amino Acids and Dipeptides as Noncovalent Hydrogels for Tissue Engineering. *Polym. Chem.* **2012**, *3*, 18−33.
(8) Adams, D. J.; Topham, P. D. Peptide Conjugate Hydrogelators. *Soft Matter* **2010**, *6*, 3707−3721.
(9) Yokoi, H.; Kinoshita, T.; Zhang, S. Dynamic Reassembly of Peptide RADA16 Nanofiber Scaffold. *Proc. Natl. Acad. Sci. U.S.A.* **2005**, *102*, 8414−8419.
(10) Rudra, J. S.; Tian, Y. F.; Jung, J. P.; Collier, J. H. A Self-Assembling Peptide Acting as an Immune Adjuvant. *Proc. Natl. Acad. Sci. U.S.A.* **2010**, *107*, 622−627.
(11) Gelain, F.; Unsworth, L. D.; Zhang, S. Slow and Sustained Release of Active Cytokines from Self-Assembling Peptide Scaffolds. *J. Controlled Release* **2010**, *145*, 231−239.
(12) Luo, Z.; Wang, S.; Zhang, S. Fabrication of Self-Assembling D-Form Peptide Nanofiber Scaffold d-EAK16 for Rapid Hemostasis. *Biomaterials* **2011**, *32*, 2013−2020.
(13) Hartgerink, J. D.; Beniash, E.; Stupp, S. I. Peptide-Amphiphile Nanofibers: A Versatile Scaffold for the Preparation of Self-Assembling Materials. *Proc. Natl. Acad. Sci. U.S.A.* **2002**, *99*, 5133−5138.
(14) Yang, Z. M.; Gu, H. W.; Fu, D. G.; Gao, P.; Lam, J. K.; Xu, B. Enzymatic Formation of Supramolecular Hydrogels. *Adv. Mater.* **2004**, *16*, 1440−1444.
(15) Smith, A. M.; Williams, R. J.; Tang, C.; Coppo, P.; Collins, R. F.; Turner, M. L.; Saiani, A.; Ulijn, R. V. Fmoc-Diphenylalanine Self Assembles to a Hydrogel *via* a Novel Architecture Based on pi-pi Interlocked Beta-Sheets. *Adv. Mater.* **2008**, *20*, 37−41.
(16) Ou, C.; Zhang, J.; Zhang, X.; Yang, Z.; Chen, M. Phenothiazine as an Aromatic Capping Group to Construct a Short Peptide-Based 'Super Gelator'. *Chem. Commun.* **2013**, *49*, 1853−1855.
(17) Fleming, S.; Debnath, S.; Frederix, P. W.; Hunt, N. T.; Ulijn, R. V. Insights into the Coassembly of Hydrogelators and Surfactants Based on Aromatic Peptide Amphiphiles. *Biomacromolecules* **2014**, *15*, 1171−1184.
(18) Jayawarna, V.; Ali, M.; Jowitt, T. A.; Miller, A. E.; Saiani, A.; Gough, J. E.; Ulijn, R. V. Nanostructured Hydrogels for Three-Dimensional Cell Culture Through Self-Assembly of Fluorenylmethoxycarbonyl-Dipeptides. *Adv. Mater.* **2006**, *18*, 611−614.
(19) Chien, M.-P.; Carlini, A. S.; Hu, D.; Barback, C. V.; Rush, A. M.; Hall, D. J.; Orr, G.; Gianneschi, N. C. Enzyme-Directed Assembly of Nanoparticles in Tumors Monitored by *in Vivo* Whole Animal Imaging and *ex Vivo* Super-Resolution Fluorescence Imaging. *J. Am. Chem. Soc.* **2013**, *135*, 18710−18713.
(20) Mizusawa, K.; Ishida, Y.; Takaoka, Y.; Miyagawa, M.; Tsukiji, S.; Hamachi, I. Disassembly-Driven Turn-on Fluorescent Nanoprobes for Selective Protein Detection. *J. Am. Chem. Soc.* **2010**, *132*, 7291−7293.
(21) Wang, H.; Liu, J.; Han, A.; Xiao, N.; Xue, Z.; Wang, G.; Long, J.; Kong, D.; Liu, B.; Yang, Z.; Ding, D. Self-Assembly-Induced Far-Red/Near-Infrared Fluorescence Light-Up for Detecting and Visualizing Specific Protein-Peptide Interactions. *ACS Nano* **2014**, *8*, 1475−1484.
(22) Zhou, M.; Smith, A. M.; Das, A. K.; Hodson, N. W.; Collins, R. F.; Ulijn, R. V.; Gough, J. E. Self-Assembled Peptide-Based Hydrogels as Scaffolds for Anchorage-Dependent Cells. *Biomaterials* **2009**, *30*, 2523−2530.
(23) McClendon, M. T.; Stupp, S. I. Tubular Hydrogels of Circumferentially Aligned Nanofibers to Encapsulate and Orient Vascular Cells. *Biomaterials* **2012**, *33*, 5713−5722.
(24) Zhao, F.; Ma, M. L.; Xu, B. Molecular Hydrogels of Therapeutic Agents. *Chem. Soc. Rev.* **2009**, *38*, 883−891.
(25) Cheetham, A. G.; Zhang, P. C.; Lin, Y. A.; Lock, L. L.; Cui, H. G. Supramolecular Nanostructures Formed by Anticancer Drug Assembly. *J. Am. Chem. Soc.* **2013**, *135*, 2907−2910.
(26) Soukasene, S.; Toft, D. J.; Moyer, T. J.; Lu, H.; Lee, H.-K.; Standley, S. M.; Cryns, V. L.; Stupp, S. I. Antitumor Activity of Peptide Amphiphile Nanofiber-Encapsulated Camptothecin. *ACS Nano* **2011**, *5*, 9113−9121.
(27) Yang, Z.; Xu, K.; Guo, Z.; Guo, Z.; Xu, B. Intracellular Enzymatic Formation of Nanofibers Results in Hydrogelation and Regulated Cell Death. *Adv. Mater.* **2007**, *19*, 3152−3156.
(28) Kuang, Y.; Xu, B. Disruption of the Dynamics of Microtubules and Selective Inhibition of Glioblastoma Cells by Nanofibers of Small Hydrophobic Molecules. *Angew. Chem., Int. Ed. Engl.* **2013**, *52*, 6944−6948.
(29) Ren, C.; Wang, H.; Zhang, X.; Ding, D.; Wang, L.; Yang, Z. Interfacial Self-Assembly Leads to Formation of Fluorescent Nanoparticles for Simultaneous Bacterial Detection and Inhibition. *Chem. Commun.* **2014**, *50*, 3473−3475.
(30) Veiga, A. S.; Sinthuvanich, C.; Gaspar, D.; Franquelim, H. G.; Castanho, M.; Schneider, J. P. Arginine-Rich Self-Assembling Peptides as Potent Antibacterial Gels. *Biomaterials* **2012**, *33*, 8907−8916.
(31) Boekhoven, J.; Stupp, S. I. 25th Anniversary Article: Supramolecular Materials for Regenerative Medicine. *Adv. Mater.* **2014**, *26*, 1642−1659.
(32) Davis, M. E.; Motion, J. P. M.; Narmoneva, D. A.; Takahashi, T.; Hakuno, D.; Kamm, R. D.; Zhang, S. G.; Lee, R. T. Injectable Self-Assembling Peptide Nanofibers Create Intramyocardial Microenvironments for Endothelial Cells. *Circulation* **2005**, *111*, 442−450.
(33) Davis, M. E.; Hsieh, P. C. H.; Takahashi, T.; Song, Q.; Zhang, S. G.; Kamm, R. D.; Grodzinsky, A. J.; Anversa, P.; Lee, R. T. Local Myocardial Insulin-Like Growth Factor 1 (IGF-1) Delivery with Biotinylated Peptide Nanofibers Improves Cell Therapy for Myocardial Infarction. *Proc. Natl. Acad. Sci. U.S.A.* **2006**, *103*, 8155−8160.
(34) Barnard, A.; Smith, D. K. Self-Assembled Multivalency: Dynamic Ligand Arrays for High-Affinity Binding. *Angew. Chem., Int. Ed.* **2012**, *51*, 6572−8581.
(35) Boekhoven, J.; Brizard, A. M.; Kowlgi, K. N.; Koper, G. J.; Eelkema, R.; van Esch, J. H. Dissipative Self-Assembly of a Molecular Gelator by Using a Chemical Fuel. *Angew. Chem., Int. Ed.* **2010**, *49*, 4825−4828.
(36) Miao, X. M.; Cao, W.; Zheng, W. T.; Wang, J. Y.; Zhang, X. L.; Gao, J.; Yang, C. B.; Kong, D. L.; Xu, H. P.; Wang, L.; Yang, Z. M. Switchable Catalytic Activity: Selenium-Containing Peptides with Redox-Controllable Self-Assembly Properties. *Angew. Chem., Int. Ed.* **2013**, *52*, 7781−7785.
(37) Wang, H. M.; Wei, J.; Yang, C. B.; Zhao, H. Y.; Li, D. X.; Yin, Z. N.; Yang, Z. M. The Inhibition of Tumor Growth and Metastasis by Self-Assembled Nanofibers of Taxol. *Biomaterials* **2012**, *33*, 5848−5853.
(38) Ghanaati, S.; Webber, M. J.; Unger, R. E.; Orth, C.; Hulvat, J. F.; Kiehna, S. E.; Barbeck, M.; Rasic, A.; Stupp, S. I.; Kirkpatrick, C. J.

DOI: 10.1021/am507800e
ACS Appl. Mater. Interfaces 2015, 7, 2735−2744

Dynamic *in Vivo* Biocompatibility of Angiogenic Peptide Amphiphile Nanofibers. *Biomaterials* **2009**, *30*, 6202−6212.
(39) Yang, Z. M.; Liang, G. L.; Ma, M. L.; Gao, Y.; Xu, B. *In Vitro* and *in Vivo* Enzymatic Formation of Supramolecular Hydrogels Based on Self-Assembled Nanofibers of a Beta-Amino Acid Derivative. *Small* **2007**, *3*, 558−562.
(40) Liang, G. L.; Yang, Z. M.; Zhang, R. J.; Li, L. H.; Fan, Y. J.; Kuang, Y.; Gao, Y.; Wang, T.; Lu, W. W.; Xu, B. Supramolecular Hydrogel of a D-Amino Acid Dipeptide for Controlled Drug Release *in Vivo*. *Langmuir* **2009**, *25*, 8419−8422.
(41) Rudra, J. S.; Sun, T.; Bird, K. C.; Daniels, M. D.; Gasiorowski, J. Z.; Chong, A. S.; Collier, J. H. Modulating Adaptive Immune Responses to Peptide Self-Assemblies. *ACS Nano* **2012**, *6*, 1557−1564.
(42) Rudra, J. S.; Mishra, S.; Chong, A. S.; Mitchell, R. A.; Nardin, E. H.; Nussenzweig, V.; Collier, J. H. Self-Assembled Peptide Nanofibers Raising Durable Antibody Responses Against a Malaria Epitope. *Biomaterials* **2012**, *33*, 6476−6484.
(43) Wu, Z. D.; Tan, M.; Chen, X. M.; Yang, Z. M.; Wang, L. Molecular Hydrogelators of Peptoid-Peptide Conjugates with Superior Stability Against Enzyme Digestion. *Nanoscale* **2012**, *4*, 3644−3646.
(44) Li, J.; Gao, Y.; Kuang, Y.; Shi, J.; Du, X.; Zhou, J.; Wang, H.; Yang, Z.; Xu, B. Dephosphorylation of D-Peptide Derivatives to Form Biofunctional, Supramolecular Nanofibers/Hydrogels and Their Potential Applications for Intracellular Imaging and Intratumoral Chemotherapy. *J. Am. Chem. Soc.* **2013**, *135*, 9907−9914.
(45) Liu, J.; Chu, L.; Zhang, Y.; Xu, H.; Kong, D.; Yang, Z.; Yang, C.; Ding, D. Self-Assembling Peptide of D-Amino Acids Boosts Selectivity and Antitumor Efficacy of 10-Hydroxycamptothecin. *ACS Appl. Mater. Interfaces* **2014**, *6*, 5558−5565.
(46) Liu, J.; Xu, H.; Zhang, Y.; Chu, L.; Liu, Q.; Song, N.; Yang, C. Novel Tumor-Targeting, Self-Assembling Peptide Nanofiber as a Carrier for Effective Curcumin Delivery. *Int. J. Nanomedicine* **2014**, *9*, 197−207.
(47) Raeburn, J.; Pont, G.; Chen, L.; Cesbron, Y.; Levy, R.; Adams, D. J. Fmoc-Diphenylalanine Hydrogels: Understanding the Variability in Reported Mechanical Properties. *Soft Matter* **2012**, *8*, 1168−1174.
(48) Shmeeda, H.; Amitay, Y.; Tzemach, D.; Gorin, J.; Gabizon, A. Liposome Encapsulation of Zoledronic Acid Results in Major Changes in Tissue Distribution and Increase in Toxicity. *J. Am. Chem. Soc.* **2013**, *167*, 265−275.
(49) Chow, T. H.; Lin, Y. Y.; Hwang, J. J.; Wang, H. E.; Tseng, Y. L.; Pang, V. F.; Liu, R. S.; Lin, W. J.; Yang, C. S.; Ting, G. Therapeutic Efficacy Evaluation of ^{111}In-Labeled PEGylated Liposomal Vinorelbine in Murine Colon Carcinoma with Multimodalities of Molecular Imaging. *J. Nucl. Med.* **2009**, *50*, 2073−2081.
(50) Garg, P. K.; Alston, K. L.; Welsh, P. C.; Zalutsky, M. R. Enhanced Binding and Inertness to Dehalogenation of α-Melanotropic Peptides Labeled Using N-Scuccinimidyl-3-Iodobenzoate. *Bioconjugate Chem.* **1996**, *7*, 233−239.
(51) Liu, Z.; Cai, W.; He, L.; Nakayama, N.; Chen, K.; Sun, X.; Chen, X.; Dai, H. *In Vivo* Biodistribution and Highly Efficient Tumour Targeting of Carbon Nanotubs in Mice. *Nat. Nanotechnol.* **2007**, *2*, 47−52.
(52) Mazza, M.; Notman, R.; Anwar, J.; Rodger, A.; Hicks, M.; Parkinson, G.; McCarthy, D.; Daviter, T.; Moger, J.; Garrett, N.; Mead, T.; Briggs, M.; Schatzlein, A. G.; Uchegbu, I. F. Nanofiber-Based Delivery of Therapeutic Peptides to the Brain. *ACS Nano* **2013**, *7*, 1016−1026.
(53) Wagh, A.; Singh, J.; Qian, S.; Law, B. A Short Circulating Peptide Nanofiber as a Carrier for Tumoral Delivery. *Nanomedicine* **2013**, *9*, 449−457.
(54) Toft, D. J.; Moyer, T. J.; Standley, S. M.; Ruff, Y.; Ugolkov, A.; Stupp, S. I.; Cryns, V. L. Coassembled Cytotoxic and PEGylated Peptide Amphiphiles Form Filamentous Nanostructures with Potent Antitumor Activity in Models of Breast Cancer. *ACS Nano* **2012**, *6*, 7956−7965.
(55) Robinson, J. T.; Hong, G.; Liang, Y.; Zhang, B.; Yaghi, O. K.; Dai, H. *In Vivo* Fluorescence Imaging in the Second Near-Infrared Window with Long Circulating Carbon Nanotubes Capable of Ultrahigh Tumor Uptake. *J. Am. Chem. Soc.* **2012**, *134*, 10664−10669.
(56) Molavi, O.; Xiong, X. B.; Douglas, D.; Kneteman, N.; Nagata, S.; Pastan, I.; Chu, Q.; Lavasanifar, A.; Lai, R. Anti-CD30 Antibody Conjugated Liposomal Doxorubicin with Significantly Improved Therapeutic Efficacy Against Anaplastic Large Cell Lymphoma. *Biomaterials* **2013**, *34*, 8718−8725.
(57) Nurunnabi, M.; Khatun, Z.; Huh, K. M.; Park, S. Y.; Lee, D. Y.; Cho, K. J.; Lee, Y. K. *In Vivo* Biodistribution and Toxicology of Carboxylated Graphene Quantum Dots. *ACS Nano* **2013**, *7*, 6858−6867.
(58) Aird, W. C. The Hematologic System as a Marker of Organ Dysfunction in Sepsis. *Mayo Clin. Proc.* **2003**, *78*, 869−881.
(59) Jung, J. P.; Nagaraj, A. K.; Fox, E. K.; Rudra, J. S.; Devgun, J. M.; Collier, J. H. Co-Assembling Peptides as Defined Matrices for Endothelial Eells. *Biomaterials* **2009**, *30*, 2400−2410.

DOI: 10.1021/am507800e
ACS Appl. Mater. Interfaces 2015, 7, 2735−2744